Distribution of resting and ligand-bound ErbB1 and ErbB2 receptor tyrosine kinases in living cells using number and brightness analysis

Peter Nagy[a,b], Jeroen Claus[a,c,2], Thomas M. Jovin[a], and Donna J. Arndt-Jovin[a,1]

[a]Laboratory of Cellular Dynamics, Max Planck Institute for Biophysical Chemistry, Am Faßberg 11, D-37077 Göttingen, Germany; [b]Department of Biophysics and Cell Biology, University of Debrecen, Nagyerdei krt. 98, H4012 Debrecen, Hungary; and [c]University College, Science Department, 3508 BE Utrecht, Netherlands

Edited* by Joseph Schlessinger, Yale University School of Medicine, New Haven, CT, and approved July 29, 2010 (received for review March 4, 2010)

Ligand-driven dimerizations of ErbB receptor subunits fulfill a fundamental role in their activation. We have used the number and brightness analysis technique to investigate the existence of preformed ligand-independent dimers and clusters and to characterize the initial steps in the activation of ErbB1 and ErbB2. In cells expressing 50,000–200,000 receptors, ErbB1 was monomeric in the absence of ligand stimulation, whereas in CHO cells with receptor levels >500,000 as much as 30% of ErbB1 was present as preformed dimers. EGF induced the formation of ErbB1 dimers as well as larger clusters (up to pentamers) that colocalized with clathrin-coated pits. The distribution of unstimulated ErbB2 in cells expressing $3{\cdot}10^5 - 10^6$ receptors was fundamentally different, in that this receptor was present in preformed homoassociated aggregates containing 5–10 molecules. These constitutive ErbB2 homoclusters colocalized with caveolae, increased in size at subphysiological temperatures, but decreased in size upon EGF stimulation. We conclude that these ErbB2 clusters are promoted primarily by membrane-mediated interactions and are dispersed upon ligand stimulation.

EGFR | epidermal growth factor | ErbB proteins | receptor clusters | signal transduction

ErbB proteins (ErbB1-4, HER1-4) constitute the best characterized family of receptor tyrosine kinases (1). Biochemical analysis has demonstrated that ErbB1, the prototypical member of the family (also known as the epidermal growth factor receptor, EGFR or HER1) undergoes ligand-induced homodimerization as a key step in its activation (2). More recent crystallographic studies reveal that ligand binding induces a transition from a closed conformation of ErbB1 to an extended configuration with the capacity to dimerize via intermolecular interactions mediated by domain II (3, 4). The ultrastructural data also confirm that dimerization of ErbB1 plays a fundamental role in activating the kinase domain by a mechanism resembling that of cyclin dependent kinases (5, 6). The coreceptor ErbB2 has no known ligand but upon transactivation expresses the most potent kinase activity of the ErbB family, thereby increasing the efficiency of signaling mediated by ErbB2-containing heterodimers (7). ErbB2 constitutively adopts an extended conformation potentiating the formation of heterodimers (8, 9) that can be inhibited by pertuzumab, a monoclonal antibody sterically blocking the heterodimerization arm of ErbB2 (10). Although the extracellular domain of ErbB2 has failed to form crystallographic homodimers, molecular biological and fluorescence resonance energy transfer (FRET) experiments have shown that full-length ErbB2 exists in dimers or higher-order aggregates in the plasma membrane (11, 12). The implication is that the transmembrane, juxtamembrane and other intracellular domains (5, 13, 14) act in conjunction with the membrane environment (15) to mediate the dimerization and, thereby, functional states of ErbB proteins.

Many investigators have sought to determine the distribution of ErbB1 in the plasma membrane in an attempt to explain the molecular basis for the apparent high- and low-affinity ligand binding. The findings suggest the existence of preformed (i.e., ligand-independent, ErbB1 receptor dimers) (16, 17) or larger aggregates (18) in addition to the classical dimers formed upon ligand-induced activation of receptor monomers. However, the different techniques, cell types, and conditions of the experiments have resulted in conflicting and contradictory results. Several studies using fixed cells and/or low temperature incubations based on hetero- or homo-FRET have indicated that <10% to as much as 50% of ErbB1 may exist as preformed dimers or oligomers (17, 19, 20). Inhibition of the tyrosine kinase activity of the receptor led to disaggregation of the transient dimers and clusters to monomers (18), suggesting that some measurements may have been made on nonstarved cells with preactivated receptors. On the other hand, fluorescence correlation spectroscopy (FCS) measurements on living, starved cells were consistent with earlier evidence for low levels of preformed dimers and very few oligomers (21). Recently, flow cytometric homo-FRET data demonstrated that homoclustering of ErbB2 was significantly stronger than ErbB1 and that homoaggregates of ErbB2, containing inactive proteins, were recruited into ErbB1- or ErbB3 containing heterodimers upon ligand binding (22).

We have utilized a new correlation method introduced by the Gratton lab (23) that directly assesses the molecular size of diffusing macromolecules in living cells by number and brightness (N&B) determinations based on the analysis of sequential confocal microscopy images acquired by calibrated single photon detection. The fluctuation of fluorescence intensities in single pixels provides a measure of molecular brightness (i.e., the number of detected photons emitted by a single diffusing unit of a given fluorescent species during the pixel dwell time). We found that ErbB1 is monomeric at low expression levels, but forms ligand-independent dimers in an expression-level and cell-type dependent manner. Binding of EGF induces a practically complete dimerization of ErbB1, with higher-order clusters primarily associated with clathrin-coated pits. On the contrary, ErbB2 forms homoclusters containing 5–10 proteins in the absence of stimulation, and these clusters are reduced in size after stimulation by EGF. In the absence of ligand the ErbB2 clusters increase in size at subphysiological temperatures. Our results resolve many of the published contradictions regarding the existence of pre-

Author contributions: P.N., T.M.J., and D.J.A.-J. designed research; P.N. and J.C. performed research; P.N. analyzed data; and P.N., T.M.J., and D.J.A.-J. wrote the paper.

The authors declare no conflict of interest.

*This Direct Submission article had a prearranged editor.

Freely available online through the PNAS open access option.

[1]To whom correspondence should be addressed. E-mail: djovin@gwdg.de.

[2]Present address: Imperial College, Department of Histopathology, Hammersmith Hospital, Du Cane Road, W12 0HS London, England.

This article contains supporting information online at www.pnas.org/lookup/suppl/doi:10.1073/pnas.1002642107/-/DCSupplemental.

formed ErbB clusters and their rearrangement after ligand stimulation and show that expression levels as well as temperature-dependent membrane rearrangements lead to significantly different receptor distributions.

Results

Preassociated ErbB1 Is Induced to Dimerize in Cells Expressing the Receptor at a High Level. The F1-4 line (transfected CHO cells stably expressing ~600,000 ErbB1-eGFP/cell (24) was used as a model system for cells overexpressing the ErbB1 receptor. Clustering of ErbB1 in starved cells was measured using the N&B approach. The distribution of brightness values was homogeneous indicating that clustering of ErbB1 did not show a steep dependence on the local density of the protein within the limited concentration range sampled on a single cell (Figs. 1*A* and 2*A*). The molecular brightness values of ErbB1-eGFP were ~30% higher than those of monomeric eGFP implying that a fraction of ErbB1 was present in preformed receptor clusters (Table 1). The existence of preformed receptor dimers in F1-4 cells was confirmed by photobleaching ~80% of the fluorescence after which the molecular brightness of ErbB1-eGFP approximated that of soluble, monomeric eGFP (Fig. 1*B* and Table 1). Stimulation of F1-4 cells by 100 nM EGF for 3 min at room temperature increased the cluster size of ErbB1 significantly (Figs. 1*A* and 2*B*) to a value that was ~80% higher than monomeric eGFP (Table 1). The brightness histogram shifted homogenously to higher values upon EGF treatment (Fig. 1*A*), but the dependence of the brightness on the fluorescence intensity was weak (Fig. 2*B* and Fig. S1*E*). These observations indicate that the growth factor induced an almost complete dimerization of the receptor population.

Preformed Clusters of ErbB1 Are Absent in Cells Expressing the Receptor at Low Levels. The observation of preformed ErbB1 clusters in unstimulated F1-4 cells might not represent the behavior of the receptor under physiological conditions due to the high overexpression in these cells. We investigated two other model systems with significantly lower levels of ErbB1 expression. F1-10 is another transfected CHO line stably expressing ~50,000 ErbB1-eGFP/cell (25), whereas the human HeLa-ErbB1eGFP line expresses ~200,000 ErbB1-eGFP/cell in a background of 50,000 endogenous, unlabeled ErbB1 receptors. The molecular brightness of ErbB1-eGFP measured in starved F1-10 and HeLa-ErbB1eGFP cells was only 3–5% higher than that of monomeric eGFP, indicating that the majority of ErbB1-eGFP was monomeric in unstimulated cells expressing moderate to low levels of the receptor (Fig. 1*C*, Fig. S1*C*, and Table 1). The brightness of ErbB1-eGFP showed a steeper dependence on its local density in F1-10 than in F1-4 cells (Fig. 2 *A* and *C*). Stimulation of both F1-10 and HeLa-ErbB1eGFP cells led to significant increases in the molecular brightness of ErbB1-eGFP (Table 1), and the distribution in EGF-stimulated F1-10 cells deviated significantly from a unimodal Gaussian (Fig. 1*C*), correlating strongly with the local density (mean fluorescence intensity) of ErbB1-eGFP (Fig. 2*C*). Larger clusters of the receptor induced by EGF (Fig. 2*D* and Fig. S1 *F* and *G*) were colocalized with clathrin-coated pits after fixation and immunfluorescence labeling (S1*H* and Figs. S2*A*). Such clusters were not observed in either quiescent or stimulated F1-4 cells (Fig. S1 *A* and *B*). Three overlapping Gaussians were required to fit the brightness distribution of EGF-stimulated F1-10 cells (Fig. 1*D*), rightmost peak corresponding to ~5 ErbB1-eGFP in clathrin-coated pits.

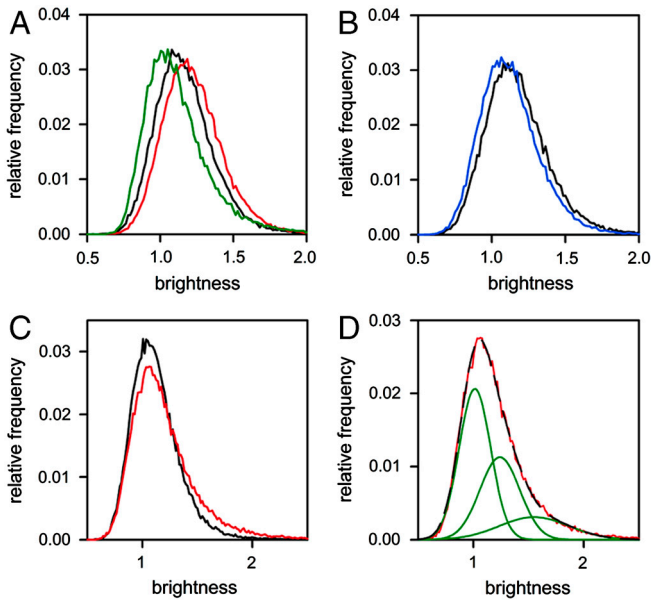

Fig. 1. Clustering of ErbB1 in quiescent and EGF-stimulated cells. (*A*). Starved F1-4 cells were measured before and after stimulation with EGF for 3 min. The brightness histograms are plotted for quiescent (black) and the EGF-stimulated cells (red). The brightness histogram of soluble monomeric eGFP is shown by the green line. (*B*). Starved F1-4 cells were photobleached until their fluorescence intensity reached ~20% of the initial value and the brightness histograms of the control (black) and the bleached cells (blue) are shown. (*C*). Brightness histograms of starved (black) and EGF-stimulated (red) F1-10 cells. (*D*). The brightness histogram of EGF-stimulated F1-10 cells (red) was fitted by three overlapping Gaussians (green lines). The sum of the three fitted Gaussian distributions perfectly overlapping the experimentally determined histogram is shown by the black, long dashed line.

The Propensity of ErbB2 to Form Homoclusters Is Greater than that of ErbB1. Starved A4erbB2 cells (26) expressing ~$1.2{\cdot}10^6$ and 10^6 endogenous ErbB1 and ErbB2-mYFP, respectively, showed remarkably heterogeneous clustering of ErbB2 both at the microscopic and molecular levels. Conspicuous "macroclusters" of ErbB2 were observed in microscopic images (Fig. S3). The molecular brightness of ErbB2-mYFP was significantly higher in these macroclusters than outside them (Figs. 3 *A* and *C* and 4 *A–D*), but the N&B analysis demonstrated that ErbB2 was homoassociated in both locations (Table 1). A similar tendency was

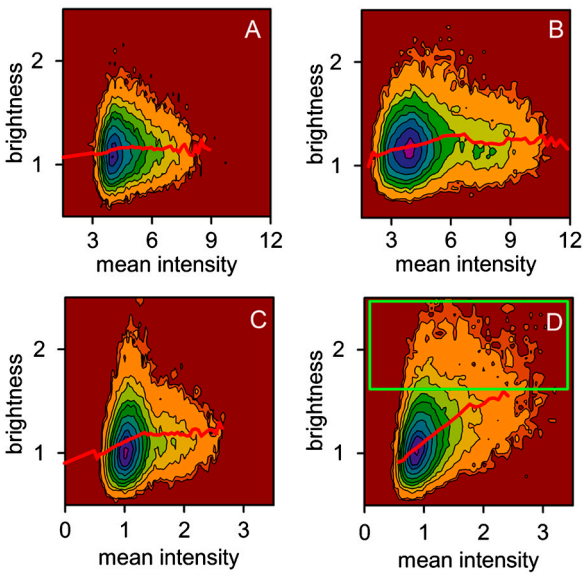

Fig. 2. N&B contour plots of quiescent and EGF-stimulated cells expressing ErbB1. N&B contour plots of starved (*A*) and EGF-stimulated (*B*) F1-4 cells, and starved (*C*) and EGF-stimulated F1-10 cells were calculated. The horizontal scales (mean fluorescence intensity) were divided into 50 bins and the average brightness calculated for each bin is shown by the red trend lines. The gated part in (*D*) marked by the green box corresponds to the gated pixels marked by red in Fig. S1*G*.

Table 1. Molecular brightness values of ErbB1-eGFP and ErbB2-mYFP

ErbB1	soluble eGFP	F1-4			F1-10		HeLa-ErbB1-eGFP	
		starved	bleached	+EGF	starved	+EGF	starved	+EGF
mol. br. (mol/cluster)	0.118 ± 0.002	0.158 ± 0.002 (1.3)	0.128 ± 0.002 (1.0)	0.217 ± 0.003 (1.8)	0.122 ± 0.001 (1.0)	0.175 ± 0.003 (1.5)	0.126 ± 0.005 (1.0)	0.172 ± 0.005 (1.5)

ErbB2	soluble mYFP		A4erbB2				CHO-ErbB2mYFP	
			starved	+EGF	pertuzumab	pertuzumab+EGF	starved	pertuzumab
mol. br. (mol/cluster)	0.063 ± 0.01	In mc	0.4 ± 0.02 (6.3)	0.283 ± 0.025 (4.5)	0.35 ± 0.023 (5.6)	0.33 ± 0.017 (5.2)	0.91 ± 0.056 (14.4)	0.75 ± 0.053 (11.9)
		outside mc	0.182 ± 0.008 (2.9)	0.164 ± 0.019 (2.6)	0.16 ± 0.021 (2.5)	0.14 ± 0.023 (2.2)	0.28 ± 0.037 (4.4)	0.28 ± 0.03 (4.4)

Molecular brightness values (±SEM) of quiescent and EGF-stimulated cells, and that of soluble, monomeric eGFP and mYFP are shown in the table. The numbers in parentheses represent the average number of ErbB1-eGFP or ErbB2-mYFP in a molecular cluster determined by dividing the molecular brightness values of cells with that of soluble monomeric fluorescent protein. The displayed values were calculated from 5–10 cells. (mc = macrocluster)

observed in CHO cells stably expressing ~300,000 ErbB2/cell but lacking the other ErbB proteins. However, in this cell line the size of molecular homoclusters of ErbB2 was even larger (Table 1), averaging 5–15 inside and 3–4 ErbB2 molecules outside the macroclusters. ErbB2-mYFP in the central and most intense part of the macroclusters had a lower molecular brightness than at the periphery (Fig. S3*A* and Fig. 4*B*). We attribute this observation to a lower mobility of ErbB2 in the central and most dense part of the clusters.

Temperature changes are expected to affect the clustering properties of integral membrane proteins that associate with specific lipid environments (15, 27, 28). Macroclusters of ErbB2 gradually increased in size and density after transferring cells from 37 °C to room temperature over a period of 2 h (Fig. S3).

Several factors might contribute to increased homoaggregation of ErbB2 compared with ErbB1: (*i*) the C-terminal PDZ binding motif that interacts with intracellular proteins such as Erbin and Pick1 (29); (*ii*) linker regions to the mYFP moiety (26); or (*iii*) the mYFP moiety itself (30). Additional transgenes were constructed: ErbB2-short-mYFP, with a dipeptide linker; ACP-ErbB2, an amino terminal acyl carrier protein (ACP) sequence insertion (31); and C-terminal VPV deletion mutants of both constructs. N&B measurements on transiently transfected HeLa cells expressing ErbB2-short-mYFP yielded data identical to those observed with the original ErbB2-mYFP vector (Fig. S4*A* and Table S1). Enzymatic covalent labeling of the ACP-ErbB2 in the plasma membrane of transfected HeLa cells with Atto-565-CoA displayed identical clustering properties to mYFP-labeled ErbB2 (Fig. S4*B* and Table S1). Finally, the cluster sizes of wild-type ErbB2 and ΔVPV-ErbB2 were not significantly different from each other in cells transfected with either mYFP-tagged or ACP-conjugated versions of the vectors (Fig. S4 *A* and *B* and Table S1). Colocalization experiments with immunolabeling

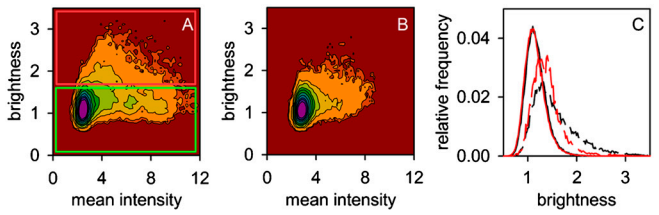

Fig. 3. N&B contour plots of quiescent and EGF-stimulated A4erbB2 cells. Starved A4erbB2 cells were stimulated with 100 nM EGF for 3 min. The N&B contour plots were calculated for the control (*A*) and EGF-stimulated cells (*B*). The top and bottom boxes in part A were used to gate pixels with high and low brightness values, respectively, and these pixels are shown in red in Fig. 4 *C* and *D*, respectively. (*C*). Brightness values separately analyzed for pixels inside (dashed line) and outside (solid line) ErbB2 macroclusters both in quiescent (black lines) and EGF-stimulated cells (red lines).

are described in *SI Text* and confirmed that no fluorescence signal contributions from internal vesicles or binding to extracellular matrix contributed to the molecular brightness determinations while macroclusters colocalize with caveolin (Fig. S5).

ErbB2 Is Removed from Preformed Homoclusters upon EGF Stimulation. A4erbB2 cells were used to measure the effect of EGF stimulation on the molecular clustering of ErbB2. EGF significantly decreased the size of molecular clusters of ErbB2 inside macroclusters without affecting external molecules (Fig. 3 *B* and *C* and Table 1). Ligand-activated ErbB1 recruited ErbB2 from homoclusters into ErbB1-2 heterodimers. Pertuzumab, an antibody blocking the heterodimerization of ErbB2, decreased the molecular brightness values of ErbB2-mYFP in starved cells and abolished the decrease induced by EGF (Table 1). We conclude that the observed EGF-induced decrease in the size of molecular homoclusters of ErbB2 was the consequence of the recruitment of ErbB2 into heterodimers by ligand-activated ErbB1.

Discussion

According to the widely accepted molecular scheme underlying the biology of ErbB receptor tyrosine kinases, inactive monomeric receptors undergo ligand-induced dimerization and activation (32). Although several lines of evidence (3, 4), support this view, both recent and earlier evidence (16–18, 20–22) have suggested that two aspects of the classical model need to be reconsidered: (*i*) inactive receptors are not necessarily monomeric, such that (*ii*) higher-order clusters of inactive and/or activated receptors may exist. We chose the novel technique of N&B analysis (23) to investigate these issues. Clusters detected by N&B analysis are defined in terms of joint mobility, whereas FRET measurements resolve aggregates based on proximity. The underlying principles of N&B and FCS measurements are the same and both measure the distribution and association states of molecules in live cells. N&B data are statistically more reliable due to the larger number of pixels used in the analysis compared with FCS. Fluorescence intensity distribution analysis and photon count histogram analysis have the potential to yield information on the distribution of cluster sizes within single pixels, something that cannot be achieved by N&B analysis. However, their requirement for highly accurate photon statistics necessitates high illumination intensities leading to photodamage (21).

The molecular brightness value of ErbB1-eGFP in unstimulated F1-4 cells expressing the receptor at a high level (>500,000/cell) was higher than that of monomeric eGFP and approached a value characteristic of preformed dimers in pixels with the highest local density. The brightness value indicated the presence of ~30% preformed dimers with no indication of higher oligomers, in agreement with previous FCS results (21). In contrast, unstimulated

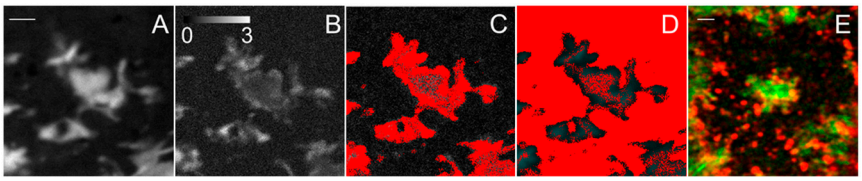

Fig. 4. Molecular brightness is different inside and outside ErbB2 macroclusters. (*A–D*). A4erbB2 cells were starved in the absence of serum, and 100 images were acquired for N&B analysis. The mean and brightness values are shown in (*A*) and (*B*), respectively. Pixels displaying high and low brightness values were gated as shown in Fig. 3, and the masks representing pixels with high (*C*) and low (*D*) brightness values were overlaid on the mean intensity image. (*E*). Starved A4erbB2 cells were fixed, permeabilized, and labeled with a monoclonal antibody against caveolin followed by secondary labeling. The fluorescence intensity of ErbB2-mYFP and the antibody against caveolin are shown in green and red, respectively. [Bars: 2 μm in (*A*), valid for (*A–D*); 1 μm in (*E*)].

ErbB1 was monomeric in two different cell lines (F1-10, HeLa-ErbB1eGFP) expressing the receptor at a lower level (50,000–200,000/cell) found on primary, nononcogenic cells. These observations suggest that the existence of preformed ErbB1 dimers is strongly dependent on the expression level and density of the receptor, and thus, may reflect the establishment of thermodynamic equilibrium. There may also be a contribution of lipid rafts and gangliosides to the tendency of ErbB1 to form preformed dimers (15, 33, 34). The fact that CHO cells do not express GM1 should also be taken into consideration (35).

Stimulation of cells with EGF led to an increase in the cluster size of ErbB1. In the high-expression F1-4 cell line the brightness histogram shifted homogeneously to larger values after EGF stimulation and the mean value of the unimodal distribution was ~1.8-times that of monomeric eGFP, demonstrating an almost complete dimerization of ErbB1 upon EGF treatment. F1-10 cells expressing ErbB1 at a much lower level (~1/10) behaved differently. The EGF-induced increase in the average molecular brightness was lower and the brightness histogram was unsymmetrical. Decomposition of the brightness histogram revealed that the main peak and the brightest subpopulation corresponded to monomeric and pentameric ErbB1, respectively. After fixation pentameric clusters could be colocalized with clathrin-coated pits by antibody labeling. We conclude that EGF-stimulation led to activation and dimerization of ErbB1 followed by immediate recruitment to clathrin-coated pits, leaving behind the remaining inactive and monomeric receptors. In F1-4 cells with high ErbB1-eGFP expression there was rapid recruitment of almost all the ErbB1 molecules into activated dimers after addition of EGF, masking the rather low number of clathrin-coated pits that were presumably saturated (36).

Whereas biochemical data (37) and X-ray crystallography (3, 4) suggest that inactive ErbB1 is monomeric, hetero-FRET (16–18), homo-FRET (19, 22, 38), and FCS (20, 21, 25) measurements have found evidence for dimers, or in a few cases for higher-order clusters. We propose that several cell- and measurement-dependent factors contribute to the discrepancies in the literature: (*i*) the strong dependence of preformed ErbB1 dimers on expression levels established in this study accounts for the presence of preformed clusters in cells (e.g., A431) with high receptor densities (16, 17); (*ii*) fixation and labeling by bivalent antibodies may artificially generate receptor aggregates (39); and (*iii*) the continuous cycle of phosphorylation and dephosphorylation of ErbB1 induced by autocrine stimulation or lack of starvation. ErbB1 is fully inactivated only in serum-deprived cells (40), and some protocols have even used phosphatase inhibitors (41), a situation promoting the formation of activated dimers. Thus, the observation of ErbB1 clusters persisting in nonstarved cells (20) leads to the erroneous conclusion that they preexist in unstimulated cells.

The perception of clusters, extending from dimers to aggregates containing hundreds of proteins (22, 42), may also reflect the size-dependent selectivity of the methods used to investigate them. Dimers observed by X-ray crystallography are direct associations on the molecular level, whereas positive FRET signals imply molecular proximity but not necessarily specific molecular interactions. Furthermore, hetero-FRET cannot discriminate between small and large aggregates, because cluster size only slightly affects the transfer efficiency (43), whereas homo-FRET is more suitable for the detection of higher-order associations (22, 38, 44). In addition, methods based on the measurement of fluorescence correlations, including N&B analysis, detect joint mobility, which can arise not only from tight molecular associations, but also by mutual confinement by membrane structures (45). The use of image correlation techniques [image correlation spectroscopy or dynamic image correlation spectroscopy (DICS)] (27, 46) to determine molecular associations applied to fixed cells is much less reliable due to fixation artifacts, photon statistics, and the optical resolution of the microscope. The overestimation of clustering or aggregate formation by DICS is apparent even in live cells from the calculated diffusion constant of $2.5{\cdot}10^{-11}$ cm^2/s for ErbB1 (27), compared to values greater by one to two orders of magnitude obtained by fluorescence recovery after photobleaching (47, 48), FCS (21, 25), and single particle tracking (49).

We propose the following model for the ErbB1 receptor, one which is in agreement with most experimental results.

- Inactive ErbB1 is monomeric when expressed at physiological, nononcogenic levels.
- Density-dependent formation of preformed clusters occurs in cells expressing the receptor at high levels. Molecules in these preformed clusters can be held together by two different types of interactions: (*i*) Mutual confinement by membrane- or cytoskeleton-mediated indirect interactions. Because lipid rafts harbor ErbB1 and influence its association state they are likely candidates for exerting the membrane-mediated confinement of ErbB1 (34, 50). The existence of preformed dimers stabilized by indirect interactions is supported by the observation of such transient protein clusters in which the distance between proteins is larger than the range of direct molecular interactions. Therefore, these clusters do not constitute stable molecular associations such as those arising after ligand binding (45). (*ii*) Direct protein–protein interactions mediated by the dimerization arm of ErbB1. It has recently been demonstrated that preformed ErbB1 dimers stabilized by their dimerization arms can arise transiently (51) but these are highly dependent upon receptor density.

ErbB2 showed a behavior strikingly different from ErbB1. In the absence of stimulation the receptors were present in preformed clusters. Microclusters of 5–15 ErbB2 receptors were found associated in larger macroclusters of ~1 μm (probably also composed of other proteins as shown in the supplementary data). Outside of these macroclusters 3–5 ErbB2 molecules were homoassociated and little monomeric protein was observed. The size of ErbB2 homoclusters was significantly larger in cells in which ErbB2 was expressed as the only member of the ErbB family (CHO-ErbB2mYFP) compared to A4erbB2 cells that coexpress $\sim 1.2{\cdot}10^6$ ErbB1 with 10^6 ErbB2-mYFP. We assume that the more extensive formation of ErbB2 homoclusters in CHO-ErbB2-

mYFP cells was due to the absence of other competing ErbB proteins. This interpretation is supported by earlier near field optical microscopy data that demonstrated larger ErbB2 clusters in a CHO cell line expressing less than 10^5 receptors/cell compared with the cluster size in MDA453 cells expressing ErbB2, ErbB3, and ErbB4, each at levels of $\sim 10^5$ (42). Macroclusters of ErbB2 colocalized with caveolin and ErbB1, a finding in accordance with the presumed raft-association of ErbB2 (15) and the colocalization of ErbB1 with caveolin in resting cells (50). EGF led to a decrease in the homoaggregation state of ErbB2 within macroclusters by recruitment and heterodimerization without significantly affecting the bulk of the ErbB2, in agreement with previous homo-FRET data (22). In polarized epithelial cells ErbB2 is targeted to the basolateral membrane by PDZ domain-containing proteins such as Erbin and may be clustered at specific sites by interaction with PICK1 (29). We eliminated the C-terminal PDZ binding sequence as well as a valine and proline-rich cloning linker to the mYFP tag with VPV deletion mutants and ACP-ErbB2 constructs. No changes in the cluster size or frequency were detected in these constructs compared with wild-type ErbB2. In addition to the PDZ binding motif several other domains of ErbB2 have been reported to contribute to its peculiar association properties, including the transmembrane domain (13) and the sequence 966–968 in the intracellular domain (52). Although not explicitly shown to be important for the homoassociation of ErbB2 the juxtamembrane domain (53) and the kinase domain (6) of ErbB1 are known to regulate dimerization; therefore the role these regions in inducing ErbB2 homocluster formation cannot be excluded. In addition, interactions of the extracellular glycosolation chains and the EGF-like domain of the membrane-bound mucin Muc-4 (54) could also promote ErbB2 homoaggregation.

We observed a time-dependent growth of ErbB2 macroclusters after a temperature shift from 37 to 20 °C. Such thermally induced increase in the clustering of ErbB1 (27) and other proteins (28) has been reported previously. The finding of temperature-dependent cluster formation of ErbB2 is in accordance with the observation of lipid phase separation in plasma membrane vesicles in the temperature range of 15–25 °C (55) and the raft association of ErbB2 (15). Because incubation at nonphysiogical temperatures can drastically alter the natural state of receptor distribution, conclusions regarding clustering of membrane proteins derived from data obtained in experiments involving long-term incubation at room temperature or even short-term incubation on ice should be treated with great caution.

In conclusion, we have shown that although inactive ErbB1 molecules dimerize in a density-dependent manner, these associations are not equivalent to the stable molecular dimers that form after ligand stimulation. ErbB2 has a much stronger propensity for homocluster formation, but is recruited away from these homoaggregates after EGF stimulation and formation of heteroassociations. Our results provide significant insights into the underlying molecular processes taking place during the initial steps of ErbB protein activation. Two-color N&B experiments (56) will reveal the composition of heteroclusters and provide unique insights into the mechanisms of potentiated signaling in cells expressing different sets of ErbB family members.

Materials and Methods

Cell Lines. All cell lines have been described previously (24–26, 38). Characterization of the expression levels are detailed in *SI Materials and Methods*. For microscopy experiments cells were cultured in 2- or 8-well coverglass chambers (Nalgene Nunc International) and stimulated with 100 nM EGF (R&D Systems) at room temperature.

Plasmids. Protocols for generating the ACP-ΔVPV-ErbB2, ErbB2-short-mYFP, and ΔVPV-ErbB2-short-mYFP are given in *SI Materials and Methods*.

Antibodies, Cell Labeling, and Fluorescence Microscopy for Colocalization. Information about the antibodies and experimental conditions for the data shown in Fig. S5 are given in *SI Materials and Methods*.

Number and Brightness Analysis. An IX81 Olympus microscope with the FluoView FV1000 confocal configuration was used to carry out number and brightness analysis according to Digman et al. (23). Live cells were analyzed at room temperature in Tyrode's buffer with 10 mM glucose and 0.1% BSA. Measurements were started immediately after removing cells from 37 °C and finished within 30 min to avoid changes in the distribution of receptors at room temperature. Image series of 50–100 single optical slices of the cell membrane adjacent to the coverslip were acquired in the pseudophoton counting mode with a pixel size of 41 nm at laser powers of 70 μW of 488 nm for eGFP, 90 μW of 514 nm for mYFP and 130 μW of 543 nm for Atto565-labeled samples. See *SI Text* for additional details concerning imaging and analysis methods.

ACKNOWLEDGMENTS. We thank an anonymous reviewer for the suggestion to remove the PDZ binding sequence of ErbB2 (C-terminal VPV segment) to assess its influence on the homoassociation of the receptors. We thank Enrico Gratton for advice concerning the N&B method. This work was supported by the Max Planck Society, FP6 STREP Grant FLUOROMAG #037465 from the European Commission, and Hungarian Scientific Research Fund Grant K72677.

1. Hynes NE, MacDonald G (2009) ErbB receptors and signaling pathways in cancer. *Curr Opin Cell Biol* 21:177–184.
2. Cochet C, et al. (1988) Demonstration of epidermal growth factor-iduced receptor dimerization in living cells using a chemical convalent cross-linking agent. *J Biol Chem* 263:3290–3295.
3. Ogiso H, et al. (2002) Crystal structure of the complex of human epidermal growth factor and receptor extracellular domains. *Cell* 110:775–787.
4. Schmiedel J, Blaukat A, Li S, Knochel T, Ferguson KM (2008) Matuzumab binding to EGFR prevents the conformational rearrangement required for dimerization. *Cancer Cell* 13:365–373.
5. Bose R, Zhang X (2009) The ErbB kinase domain: structural perspectives into kinase activation and inhibition. *Exp Cell Res* 315:649–658.
6. Zhang X, Gureasko J, Shen K, Cole PA, Kuriyan J (2006) An allosteric mechanism for activation of the kinase domain of epidermal growth factor receptor. *Cell* 125:1137–1149.
7. Klapper LN, et al. (1999) The ErbB-2/HER2 oncoprotein of human carcinomas may function solely as a shared coreceptor for multiple stroma-derived growth factors. *Proc Natl Acad Sci USA* 96:4995–5000.
8. Cho HS, et al. (2003) Structure of the extracellular region of HER2 alone and in complex with the Herceptin Fab. *Nature* 421:756–760.
9. Garrett TP, et al. (2003) The crystal structure of a truncated ErbB2 ectodomain reveals an active conformation, poised to interact with other ErbB receptors. *Mol Cell* 11:495–505.
10. Franklin MC, et al. (2004) Insights into ErbB signaling from the structure of the ErbB2-pertuzumab complex. *Cancer Cell* 5:317–328.
11. Nagy P, et al. (1998) EGF-induced redistribution of erbB2 on breast tumor cells: flow and image cytometric energy transfer measurements. *Cytometry* 32:120–131.
12. Worthylake R, Opresko LK, Wiley HS (1999) ErbB-2 amplification inhibits down-regulation and induces constitutive activation of both ErbB-2 and epidermal growth factor receptors. *J Biol Chem* 274:8865–8874.
13. Duneau JP, Vegh AP, Sturgis JN (2007) A dimerization hierarchy in the transmembrane domains of the HER receptor family. *Biochemistry* 46:2010–2019.
14. McLaughlin S, Smith SO, Hayman MJ, Murray D (2005) An electrostatic engine model for autoinhibition and activation of the epidermal growth factor receptor (EGFR/ErbB) family. *J Gen Physiol* 126:41–53.
15. Nagy P, et al. (2002) Lipid rafts and the local density of ErbB proteins influence the biological role of homo- and heteroassociations of ErbB2. *J Cell Sci* 115:4251–4262.
16. Gadella TW, Jr, Jovin TM (1995) Oligomerization of epidermal growth factor receptors on A431 cells studied by time-resolved fluorescence imaging microscopy. A stereochemical model for tyrosine kinase receptor activation. *J Cell Biol* 129:1543–1558.
17. Martin-Fernandez M, Clarke DT, Tobin MJ, Jones SV, Jones GR (2002) Preformed oligomeric epidermal growth factor receptors undergo an ectodomain structure change during signaling. *Biophys J* 82:2415–2427.
18. Clayton AH, Tavarnesi ML, Johns TG (2007) Unligated epidermal growth factor receptor forms higher order oligomers within microclusters on A431 cells that are sensitive to tyrosine kinase inhibitor binding. *Biochemistry* 46:4589–4597.
19. Bader AN, Hofman EG, Voortman J, van Bergen En Henegouwen PM, Gerritsen HC (2009) Homo-FRET imaging enables quantification of protein cluster sizes with subcellular resolution. *Biophys J* 97:2613–2622.
20. Liu P, et al. (2007) Investigation of the dimerization of proteins from the epidermal growth factor receptor family by single wavelength fluorescence cross-correlation spectroscopy. *Biophys J* 93:684–698.

21. Saffarian S, Li Y, Elson EL, Pike LJ (2007) Oligomerization of the EGF receptor investigated by live cell fluorescence intensity distribution analysis. *Biophys J* 93:1021–1031.
22. Szabó A, Horváth G, Szöllősi J, Nagy P (2008) Quantitative characterization of the large-scale association of ErbB1 and ErbB2 by flow cytometric homo-FRET measurements. *Biophys J* 95:2086–2096.
23. Digman MA, Dalal R, Horwitz AF, Gratton E (2008) Mapping the number of molecules and brightness in the laser scanning microscope. *Biophys J* 94:2320–2332.
24. Brock R, Hamelers IH, Jovin TM (1999) Comparison of fixation protocols for adherent cultured cells applied to a GFP fusion protein of the epidermal growth factor receptor. *Cytometry* 35:353–362.
25. Brock R, Jovin TM (2001) Fluorescence correlation microscopy (FCM): Fluorescence correlation spectroscopy (FCS) in cell biology. *Fluorescence Correlation Spectroscopy: Theory and Applications*, eds R Rigler and EL Elson (Springer–Verlag, Berlin), Vol 65, pp 132–161.
26. Lidke DS, et al. (2004) Quantum dot ligands provide new insights into erbB/HER receptor-mediated signal transduction. *Nat Biotechnol* 22:198–203.
27. Keating E, Nohe A, Petersen NO (2007) Studies of distribution, location, and dynamic properties of EGFR on the cell surface measured by image correlation spectroscopy. *Eur Biophys J* 37:469–481.
28. Seeger HM, Bortolotti CA, Alessandrini A, Facci P (2009) Phase-transition-induced protein redistribution in lipid bilayers. *J Phys Chem B* 113:16654–16659.
29. Jaulin-Bastard F, et al. (2001) The ERBB2/HER2 receptor differentially interacts with ERBIN and PICK1 PSD-95/DLG/ZO-1 domain proteins. *J Biol Chem* 276:15256–15263.
30. Shi X, et al. (2007) Anomalous negative fluorescence anisotropy in yellow fluorescent protein (YFP 10C): Quantitative analysis of FRET in YFP dimers. *Biochemistry* 46:14403–14417.
31. Vivero-Pol L, George N, Krumm H, Johnsson K, Johnsson N (2005) Multicolor imaging of cell surface proteins. *J Am Chem Soc* 127:12770–12771.
32. Lemmon MA (2009) Ligand-induced ErbB receptor dimerization. *Exp Cell Res* 315:638–648.
33. Lingwood D, Kaiser HJ, Levental I, Simons K (2009) Lipid rafts as functional heterogeneity in cell membranes. *Biochem Soc Trans* 37:955–960.
34. Miljan EA, Bremer EG (2002) Regulation of growth factor receptors by gangliosides. *Sci STKE* 2002:RE15.
35. Kovács T, Kárász A, Szöllősi J, Nagy P (2009) The density of GM1-enriched lipid rafts correlates inversely with the efficiency of transfection mediated by cationic liposomes. *Cytometry A* 75:650–657.
36. Sorkin A, Goh LK (2009) Endocytosis and intracellular trafficking of ErbBs. *Exp Cell Res* 315:683–696.
37. Yarden Y, Schlessinger J (1987) Epidermal growth factor induces rapid, reversible aggregation of the purified epidermal growth factor receptor. *Biochemistry* 26:1443–1451.
38. Lidke DS, et al. (2003) Imaging molecular interactions in cells by dynamic and static fluorescence anisotropy (rFLIM and emFRET). *Biochem Soc Trans* 31:1020–1027.
39. Kusumi A, Suzuki K (2005) Toward understanding the dynamics of membrane-raft-based molecular interactions. *Biochim Biophys Acta* 1746:234–251.
40. Offterdinger M, Georget V, Girod A, Bastiaens PI (2004) Imaging phosphorylation dynamics of the epidermal growth factor receptor. *J Biol Chem* 279:36972–36981.
41. Clayton AH, Orchard SG, Nice EC, Posner RG, Burgess AW (2008) Predominance of activated EGFR higher-order oligomers on the cell surface. *Growth Factors* 26:316–324.
42. Nagy P, et al. (1999) Activation-dependent clustering of the erbB2 receptor tyrosine kinase detected by scanning near-field optical microscopy. *J Cell Sci* 112:1733–1741.
43. Anikovsky M, Dale L, Ferguson S, Petersen N (2008) Resonance energy transfer in cells: A new look at fixation effect and receptor aggregation on cell membrane. *Biophys J* 95:1349–1359.
44. Yeow EK, Clayton AH (2007) Enumeration of oligomerization states of membrane proteins in living cells by homo-FRET spectroscopy and microscopy: Theory and application. *Biophys J* 92:3098–3104.
45. Andrews NL, et al. (2008) Actin restricts FceRI diffusion and facilitates antigen-induced receptor immobilization. *Nat Cell Biol* 10:955–963.
46. Clayton AH, et al. (2005) Ligand-induced dimer-tetramer transition during the activation of the cell surface epidermal growth factor receptor—A multidimensional microscopy analysis. *J Biol Chem* 280:30392–30399.
47. Lidke DS, Lidke KA, Rieger B, Jovin TM, Arndt-Jovin DJ (2005) Reaching out for signals: Filopodia sense EGF and respond by directed retrograde transport of activated receptors. *J Cell Biol* 170:619–626.
48. Zidovetzki R, Yarden Y, Schlessinger J, Jovin TM (1981) Rotational diffusion of epidermal growth factor complexed to cell surface receptors reflects rapid microaggregation and endocytosis of occupied receptors. *Proc Natl Acad Sci USA* 78:6981–6985.
49. Kusumi A, Sako Y, Yamamoto M (1993) Confined lateral diffusion of membrane receptors as studied by single particle tracking (nanovid microscopy). Effects of calcium-induced differentiation in cultured epithelial cells. *Biophys J* 65:2021–2040.
50. Mineo C, Gill GN, Anderson RG (1999) Regulated migration of epidermal growth factor receptor from caveolae. *J Biol Chem* 274:30636–30643.
51. Chung I, et al. (2010) Spatial control of EGF receptor activation by reversible dimerization on living cells. *Nature* 464:783–787.
52. Penuel E, Akita RW, Sliwkowski MX (2002) Identification of a region within the ErbB2/HER2 intracellular domain that is necessary for ligand-independent association. *J Biol Chem* 277:28468–28473.
53. Jura N, et al. (2009) Mechanism for activation of the EGF receptor catalytic domain by the juxtamembrane segment. *Cell* 137:1293–1307.
54. Kozloski GA, Carraway CA, Carraway KL (2010) Mechanistic and signaling analysis of Muc4-ErbB2 signaling module: new insights into the mechanism of ligand-independent ErbB2 activity. *J Cell Physiol* 224:649–657.
55. Veatch SL, et al. (2008) Critical fluctuations in plasma membrane vesicles. *ACS Chem Biol* 3:287–293.
56. Digman MA, Wiseman PW, Choi C, Horwitz AR, Gratton E (2009) Stoichiometry of molecular complexes at adhesions in living cells. *Proc Natl Acad Sci USA* 106:2170–2175.

Supporting Information

Nagy et al. 10.1073/pnas.1002642107

SI Text

SI Results. ***Determination of molecular brightness and cluster size for ErbB2-short-mYFP or ACP-ErbB2 transfected HeLa cells.*** The PDZ domain binding motif (VPV) was deleted from ErbB2-short-mYFP and ACP-ErbB2, and HeLa cells were transfected with plasmids coding for the ΔVPV-deletion mutants or wild-type ErbB2-short-mYFP or ACP-ErbB2 respectively. Cells expressing ACP-tagged ErbB2 were labeled with Atto565 using Sfp transferase two days after transfection. Atto565-labeled and mYFP-expressing cells were analyzed by the N&B method (Fig. S4). The molecular brightness of ErbB2 was analyzed inside and outside macroclusters and the means ± standard errors of ∼10 cells are displayed in Table S1. The molecular brightness of soluble monomeric fluorophores was also determined. To determine the average number of ErbB2 molecules in a molecular cluster (displayed in parentheses, Table S1) cellular molecular brightness values were divided by that of the soluble fluorophore. Because HeLa cells express ∼30,000 endogenous ErbB2, these numbers had to be corrected for the presence of "dark," unlabeled ErbB2. The total number of ErbB2 in transfected cells was $\sim 5 \cdot 10^5$ and $\sim 3 \cdot 10^5$ in the case of cells transfected with mYFP- and ACP-tagged proteins, respectively (numbers determined by Qifikit). Therefore, the number of molecules/cluster was divided by 0.94 and 0.9 in the two cases. In cells expressing ACP-tagged proteins a further correction was necessary to account for the incomplete labeling of the ACP-tag by Sfp transferase. It was determined in a separate experiment that ∼60% saturation of the ACP-tag is achieved with 5 μM Atto565-CoA; therefore the number of molecules/cluster was divided by 0.6. The data shown in Table S1 and Fig. S4 show conclusively that the high potential for ErbB2 to form clusters is independent of the C-terminal PDZ binding sequence and not influenced by the mYFP moiety.

Colocalization analysis of ErbB2 with membrane components and/or internal vesicles. We eliminated potential artifacts arising from internal vesicles or receptor binding to the extracellular matrix as causes of increased molecular brightness in ErbB2 cells by colocalization experiments. Upon labeling intact cells with a fluorescent antibody against the extracellular portion of ErbB2, a strong correlation between the antibody and the ErbB2-mYFP signals was observed, confirming that ErbB2 homoclusters reside in the plasma membrane and internal vesicles do not contribute to the observed signal (Fig. S5 *A* and *B*). Furthermore, there was no colocalization between ErbB2 macroclusters and focal contacts (Fig. S5 *C* and *D*), clathrin-coated pits (Fig. S5 *E* and *F*) or endocytic vesicles (Fig. S5 *G* and *H*). However, labeling of caveolin revealed a significant degree of colocalization with ErbB2 macroclusters (Fig. S2*B* and Fig. 4*E*). Although the correlation coefficient was intermediate in value ($r = 0.5$), visual inspection of the images revealed a tendency of ErbB2 macroclusters to be surrounded by caveolae (Fig. 4*E*). This observation suggests that the colocalization is driven more by the local membrane environment around caveolae rather than a specific association of ErbB2 with caveolin itself. ErbB1 was also found to colocalize with ErbB2 macroclusters (Fig. S5 *I* and *J*).

SI Materials and Methods. ***ErbB expression levels in stably transfected cell lines.*** The CHO clones, designated F1-4 and F1-10 (1, 2), express $\sim 6 \cdot 10^5$ and $\sim 5 \cdot 10^4$ ErbB1-eGFP/cell, respectively. Expression levels were characterized by flow cytometry using Qifikit (Dako-Cytomation, DAKO). HeLa-ErbB1eGFP cells express $\sim 2 \cdot 10^5$ ErbB1-eGFP/cell (3). The cells, designated A4erbB2, express $\sim 1 \cdot 10^6$ ErbB2-mYFP/cell and $\sim 2 \cdot 10^4$ endogenous ErbB2 (4). A4erbB2 cells express $\sim 1.2 \cdot 10^6$ endogenous ErbB1/cell. CHO cells express endogenous ErbB proteins at a level undetectable by flow cytometry or Western blot. The cell line, designated CHO-ErbB2mYFP, expresses $\sim 3 \cdot 10^5$ ErbB2-mYFP/cell (5). For microscopy experiments cells were cultured in 2- or 8-well coverglass chambers (NalgeneNunc International) and stimulated with 100 nM EGF (R&D Systems) at room temperature.

Plasmids, transfection. A 21 amino acid acyl carrier protein (ACP) sequence mt1.3 was derived by Natalie George (6) through mutagenesis and selection from the full length *Escherichia coli* ACP. To generate ACP-ErbB2, which can be labeled by Sfp transferase, this sequence was inserted after residue 23 of the signal peptide of the ErbB2 ORF by In-Fusion cloning into an EcoRV digest of pcDNA3-ErbB2 with the following oligonucleotide sequence: TTTTGGTGGGGCCTGGATTCCCTGGATACCGTG-GAACTGGTGATGGCGCTGGAAGAAGAATTT. The ΔVPV deletion mutant (ΔVPV-ACP-ErbB2) was created by PCR of the ACP-ErbB2 ORF and ligated into pcDNA3 with Not1 and Xba1 at the 5′ and 3′ ends, respectively. The wild-type and mutant ErbB2 plasmids were confirmed by sequencing.

The original ErbB2mYFP (A206K) in the pEYFP N1 vector has a long, 19 amino acid linker sequence containing several valine and proline residues (4). To eliminate any possible influence of either the linker or the terminal VPV amino acids in ErbB2 we recloned the wild-type ErbB2 and ΔVPV-ErbB2 with Nhe1/HindIII into mYFP pcDNA3.1zeo+ (mYFP inserted HindIII toXhoI). The names of the resultant vectors are ErbB2-short-mYFP and ΔVPV-ErbB2-short-mYFP. This strategy results in only a lysine-leucine dipeptide linker from the HindIII site between ErbB2 and the mYFP sequence.

For transfection ∼1 million HeLa cells were electroporated by the Nucleofector device of Lonza using 2 μg plasmid DNA, solution R, and program I-013.

Isolation of Sfp transferase, synthesis of Atto565-CoA and labeling of cells expressing ACP-tagged ErbB2 using Sfp transferase. Sfp phosphopantetheinyl transferase-His_6 enzyme was purified from pET29-Sfp (the kind gift of Jun Yin, Harvard Medical School) according to author's protocol (7). Atto565-CoA was synthesized from Atto565-maleimide (Atto-Tec GmbH) and CoA dilithium salt (Sigma–Aldrich) according to published protocols (7, 8) and purified on a C18 column by HPLC with an acetonitrile/ammonium acetate gradient. ACP-ErbB2 was labeled in the membrane of expressing cells with 0.2 μM Sfp transferase and 5 μM Atto565-CoA in the presence of 10 mM $MgCl_2$ in Tyrode's buffer for 20 min at room temperature followed by washing and subsequent N&B analysis of the cells.

Antibodies, cell labeling, and fluorescence microscopy for colocalization experiments. Mab528, a monoclonal antibody against the extracellular portion of ErbB1, was prepared from the supernatant of the HB-8509 hybridoma cell line obtained from ATCC. The anti-ErbB2 antibody, trastuzumab, was purchased from Roche Ltd. Mab528 and trastuzumab were labeled with AlexaFluor647 (Invitrogen–Molecular Probes) according to the manufacturer's specifications. ErbB1 phosphorylated at Tyr1068 and the light chain of clathrin were detected with the mouse monoclonal antibody 2236L (Cell Signaling) and CON.1 (Dianova), respectively. α-actinin and caveolin were labeled with rabbit polyclonal anti-

bodies (α-actinin: A2543, Sigma–Aldrich; caveolin: ab18199, Abcam). Cells were fixed in 3.7% formaldehyde for 30 min on ice and labeled with the primary antibodies in permeabilization buffer (PBS containing 0.1% (v/v) Triton X-100 and 1 mg/mL BSA) for 30 min followed by secondary labeling with Cy5-conjugated anti-mouse or anti-rabbit IgG.

To investigate the uptake of transferrin cells were starved of iron in iron poor Medium 199 for 24 h and subsequently incubated in the presence of 10 μg/mL AlexaFluor633-conjugated holotransferrin (Invitrogen–Molecular Probes) for 30 min at 37 °C.

Number and brightness analysis. An IX81 Olympus microscope with the FluoView FV1000 confocal configuration was used to carry out number and brightness analysis according to Digman et al. (9). Live cells were analyzed at room temperature in Tyrode's buffer with 10 mM glucose and 0.1% BSA. Measurements were started immediately after removing cells from 37 °C and finished within 30 min to avoid changes in the distribution of receptors at room temperature. Image acquisition was performed in the pseudophoton counting mode with an UPlanSApo 60× (NA = 1.35) objective. The pixel dwell and frame times were 10 μs and 3.26 s, respectively, for imaging transfected cells, or 2 μs and 1.1 s, respectively, for imaging soluble eGFP, mYFP, or Attot565. eGFP and mYFP were excited at 488 and 514 nm, respectively, using an AOF-adjusted laser intensity of 0.1% corresponding to ∼70 and ∼90 μW, respectively, delivered to the sample. Atto565 was excited at 543 nm using a laser intensity of 130 μW measured at the sample. A single frame consisted of 512 × 512 pixels and the pixel size in the x and y directions was 41 nm. The central part of the images was used for analysis to eliminate artifacts arising from scanner speed nonlinearity at the borders. A single optical slice containing the membrane adjacent to the glass coverslip was imaged 50–100 times. The image stack was analyzed using a custom-written Matlab program (Mathworks Inc.) incorporating functions of the DipImage toolbox (Delft University of Technology). The images were first registered (i.e., corrected for lateral shift) using the correctshift function of DipImage. Then, the mean fluorescence intensity of every slice was determined. Next, the pixel variance taken along the 3rd axis (i.e., the temporal dimension was calculated as a function of the number of slices in the stack). If the mean decreased by more than 10% due to stage shift or photobleaching or if the pixel variance did not converge to zero with increasing stack size, the stack was discarded. The apparent brightness (B) and the molecular brightness (ε) of each pixel was calculated according to the following equation:

$$B = \frac{\sigma^2}{\langle k \rangle} = \varepsilon + 1$$

where σ^2 and $\langle k \rangle$ are the variance and mean, respectively, of a given pixel signal.

1. Brock R, Hamelers IH, Jovin TM (1999) Comparison of fixation protocols for adherent cultured cells applied to a GFP fusion protein of the epidermal growth factor receptor. *Cytometry* 35:353–362.
2. Brock R, Jovin TM (2001) Fluorescence correlation microscopy (FCM): Fluorescence correlation spectroscopy (FCS) in cell biology. *Fluorescence Correlation Spectroscopy: Theory and Applications*, eds Rigler R, Elson EL (Springer, Berlin), Vol 65, pp 132–161.
3. Waterman H, et al. (2002) A mutant EGF-receptor defective in ubiquitylation and endocytosis unveils a role for Grb2 in negative signaling. *EMBO J* 21:303–313.
4. Lidke DS, et al. (2004) Quantum dot ligands provide new insights into erbB/HER receptor-mediated signal transduction. *Nat Biotechnol* 22:198–203.
5. Lidke DS, et al. (2003) Imaging molecular interactions in cells by dynamic and static fluorescence anisotropy (rFLIM and emFRET). *Biochem Soc T* 31:1020–1027.
6. George N (2006) A new method for protein labeling with small molecules based on acyl carrier protein. PhD thesis (Ecole Polytechnique Féderal, Lausanne).
7. Yin J, Lin AJ, Golan DE, Walsh CT (2006) Site-specific protein labeling by Sfp phosphopantetheinyl transferase. *Nat Protoc* 1:280–285.
8. Vivero-Pol L, George N, Krumm H, Johnsson K, Johnsson N (2005) Multicolor imaging of cell surface proteins. *J Am Chem Soc* 127:12770–12771.
9. Digman MA, Dalal R, Horwitz AF, Gratton E (2008) Mapping the number of molecules and brightness in the laser scanning microscope. *Biophys J* 94:2320–2332.

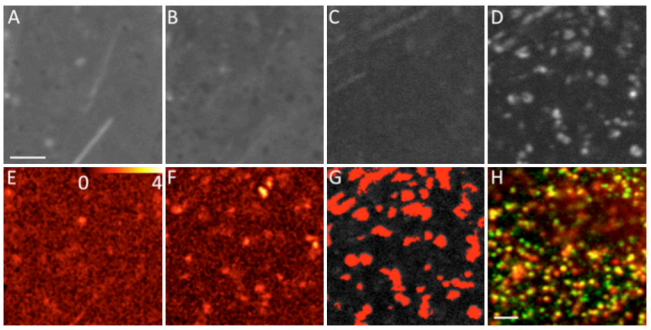

Fig. S1. Mean fluorescence and calculated brightness images of ErbB1 in quiescent and EGF-stimulated cells. (*A*–*D*). Mean fluorescence intensity images for F1-4 cells (*A*, *B*) and F1-10 cells (*C*, *D*). One hundred fluorescence images were recorded for the N&B analysis, and the mean fluorescence images of the starved (*A*, *C*) and EGF-stimulated cells (*B*, *D*) are shown. (*E*–*F*). Brightness values in F1-4 (*E*) and F1-10 cells (*F*) stimulated by EGF for 3 min shown on a pixel-by-pixel basis. (*G*). Pixels displaying high brightness values in EGF-stimulated F1-10 cells marked by red. These pixels are within the gate in Fig. 2*D*. (*H*). Colocalization between ErbB1-eGFP (green) and coated pits (red). F1-10 cells stimulated with EGF for 10 min were fixed, permeabilized and labeled by a monoclonal antibody against the light chain of clathrin followed by labeling with a Cy5-tagged secondary antibody. The bar in part A corresponds to 2 μm, and is valid for A-G. The bar in H is also 2 μm.

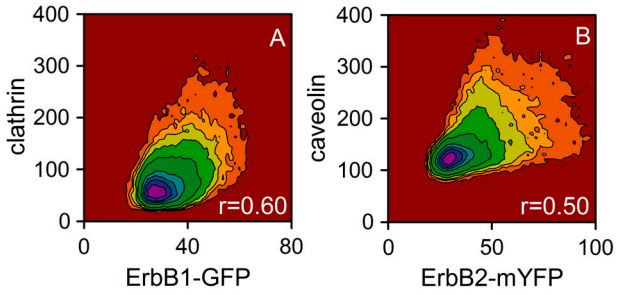

Fig. S2. Colocalization between ErbB1 and clathrin, and ErbB2 and caveolin. Two dimensional histograms showing the correlation between the fluorescence intensities of ErbB1-eGFP vs. clathrin (*A*) and ErbB2-mYFP vs. caveolin (*B*) were calculated. F1-10 cells were stimulated with 100 nM EGF for 5 min, fixed in 3.7% formaldehyde, permeabilized, and immune-labeled for coated pits with mAb against the light chain of clathrin (*A*). Starved A4erbB2 cells were labeled for caveolin by secondary immunofluorescence (*B*). The correlation coefficients (r) are also displayed in the figure. The corresponding fluorescence images are shown in Fig. S1*H* and Fig. 4*E*.

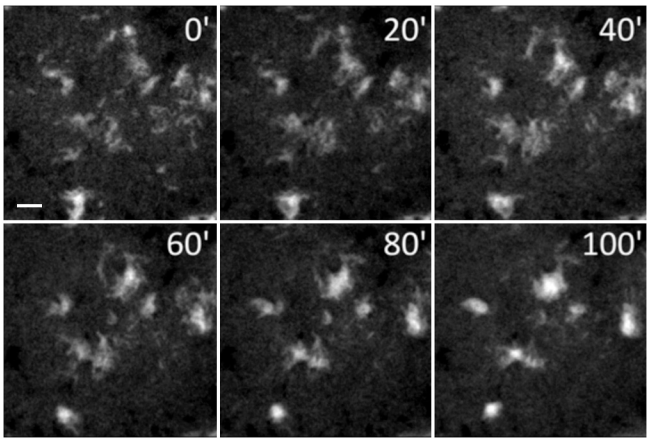

Fig. S3. Large-scale ErbB2 clusters grow at room temperature. A4erbB2 cells were starved in the absence of serum, and the same area of a single cell kept at room temperature was imaged in the confocal microscope at the indicated time points. The bar corresponds to 2 μm.

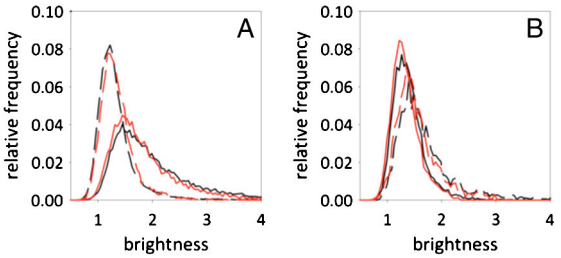

Fig. S4. The high cluster forming potential of ErbB2 is independent of the PDZ domain binding motif and the mYPF tag. A.HeLa cells were transfected with ErbB2-short-mYFP (black lines) or ΔVPV-ErbB2-short-mYFP (red lines) and N&B analysis was carried out two days after transfection. Brightness was determined inside (dashed lines) and outside (continuous lines) macroclusters of ErbB2. (*B*). HeLa cells were transfected with ACP-ErbB2 (black lines) or ACP-ΔVPV-ErbB2 (red lines), labeled with Atto565 two days after transfection and analyzed using the N&B method. Brightness was determined inside (dashed lines) and outside (continuous lines) macroclusters or ErbB2.

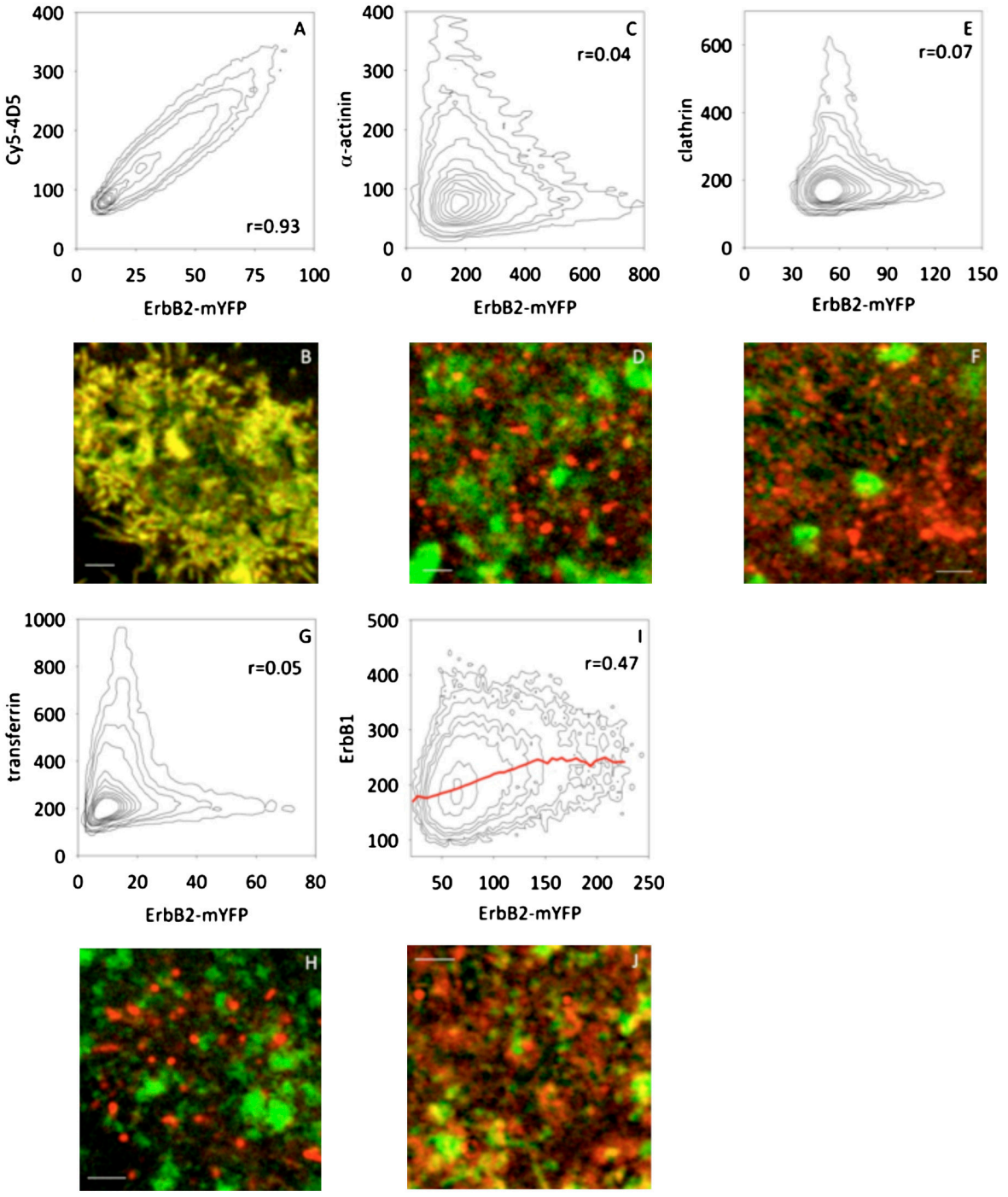

Fig. S5. Colocalization analyses of A4erbB2 cells. (*A*, *B*). Starved A4erbB2 cells were labeled with Cy5-tagged trastuzumab against ErbB2 without permeabilization. (*C–F*). Starved A4erbB2 cells were fixed, permeabilized and labeled with fluorescent antibodies against α-actinin (*C*, *D*) or clathrin light chain (*E*, *F*). (*G–H*). Starved A4erbB2 cells were incubated in the presence of fluorescent transferrin and fluorescence images of ErbB2-mYFP and transferrin were recorded. (*I*, *J*). Starved A4erbB2 cells were labeled with Cy5-tagged Mab528 (against ErbB1) without permeabilization. The red trend line shows the mean ErbB1 intensity corresponding to a given ErbB2-mYFP fluorescence intensity.The green and red intensities in the fluorescence images correspond to ErbB2-mYFP and the fluorescent antibody, respectively. The correlation between the green and red fluorescence intensities is displayed above the fluorescence images as contour plots. The correlation coefficients (r) are displayed in each contour plot. (Bars: B—3 μm; D—4 μm; F—2 μm; H—2.5 μm; J—2 μm)

Table S1. Molecular brightness of Atto565-labeled ACP-ErbB2 and ErbB2-mYFP in wild-type and ΔVPV-ErbB2

	Soluble mYFP		Wild-type ErbB2-short-mYFP	ΔVPV-ErbB2-short-mYFP
Mol. brightness (mol/cluster)	0.063 ± 0.01	Inside macroclusters	0.89 ± 0.06 (14.1)	0.96 ± 0.08 (15.2)
		Outside macroclusters	0.38 ± 0.05 (6.0)	0.4 ± 0.04 (6.4)
	Soluble Atto565		Wild-type ACP-ErbB2	ΔVPV-ACP-ErbB2
Mol. brightness (mol/cluster)	0.19 ± 0.01	Inside macroclusters	0.81 ± 0.04 (7.8)	0.76 ± 0.04 (7.3)
		Outside macroclusters	0.44 ± 0.03 (4.2)	0.39 ± 0.04 (3.7)

The PDZ domain binding motif (VPV) was deleted from ErbB2-short-mYFP and ACP-ErbB2, and HeLa cells were transfected with plasmids coding for the ΔVPV-deletion mutants or wild-type ErbB2-short-mYFP or ACP-ErbB2 respectively. Cells expressing ACP-tagged ErbB2 were labeled with Atto565 using Sfp transferase two days after transfection and Atto565-labeled and mYFP-expressing cells were analyzed by the N&B method. The molecular brightness of ErbB2 was analyzed inside and outside macroclusters and the means ± standard errors of ~10 cells are displayed. The molecular brightness of soluble monomeric fluorophores was also determined. To determine the average number of ErbB2 molecules in a molecular cluster (displayed in parentheses) cellular molecular brightness values were divided by that of the soluble fluorophore. Because HeLa cells express ~30,000 endogenous ErbB2, these numbers had to be corrected for the presence of dark, unlabeled ErbB2. The total number of ErbB2 in transfected cells was $\sim 5 \cdot 10^5$ and $\sim 3 \cdot 10^5$ in the case of cells transfected with mYFP- and ACP-tagged proteins, respectively (numbers determined by Qifikit). Therefore, the number of molecules/cluster was divided by 0.94 and 0.9 in the two cases. In cells expressing ACP-tagged proteins a further correction was necessary to account for the incomplete labeling of the ACP-tag by Sfp transferase. It was determined in a separate experiment that ~60% saturation of the ACP-tag is achieved with 5 μM Atto565-CoA; therefore the number of molecules/cluster was divided by 0.6.